



CHORUS

This is the accepted manuscript made available via CHORUS. The article has been published as:

Universal spin dynamics in quantum wires

E. A. Fajardo, U. Zülicke, and R. Winkler

Phys. Rev. B **96**, 155304 — Published 13 October 2017

DOI: [10.1103/PhysRevB.96.155304](https://doi.org/10.1103/PhysRevB.96.155304)

Universal Spin Dynamics in Quantum Wires

E. A. Fajardo,^{1,*} U. Zülicke,² and R. Winkler^{1,3}

¹*Department of Physics, Northern Illinois University, DeKalb, IL 60115, USA*

²*School of Chemical and Physical Sciences and MacDiarmid Institute for Advanced Materials and Nanotechnology, Victoria University of Wellington, PO Box 600, Wellington 6140, New Zealand*

³*Materials Science Division, Argonne National Laboratory, Argonne, IL 60439, USA*

We discuss the universal spin dynamics in quasi one-dimensional systems including the real spin in narrow-gap semiconductors like InAs and InSb, the valley pseudo-spin in staggered single-layer graphene, and the combination of real spin and valley pseudospin characterizing single-layer transition metal dichalcogenides (TMDCs) such as MoS₂, WS₂, MoS₂, and WSe₂. All these systems can be described by the same Dirac-like Hamiltonian. Spin-dependent observable effects in one of these systems thus have counterparts in each of the other systems. Effects discussed in more detail include equilibrium spin currents, current-induced spin polarization (Edelstein effect), and spin currents generated via adiabatic spin pumping. Our work also suggests that a long-debated spin-dependent correction to the position operator in single-band models should be absent.

I. INTRODUCTION

Spintronics seeks to exploit the spin degree of freedom in order to achieve new or more efficient functionalities not available in charge-based electronics.^{1–3} The spin degree of freedom emerges from a relativistic treatment of the electrons' motion. The electrons' spin interacts with the orbital environment via spin-orbit (SO) coupling that scales with the atomic number Z of the atoms involved, so that it is advantageous to use high- Z materials. On the other hand, spin-orbit coupling in novel 2D materials such as graphene with $Z = 6$ is found to be negligible.⁴

In many materials the electrons near the Fermi energy reside in multiple inequivalent valleys, which give rise to yet another degree of freedom called the valley pseudospin,^{5–9} and valleytronics seeks to exploit the valley pseudospin for new device functionalities.¹⁰ A major advantage of valleytronics over spintronics lies in the fact that it allows one to reach parameter regimes not available for the real spin in, e.g., low- Z materials such as graphene.

Previous work has touched on the conceptual similarities between, on the one hand, the real spin and spin-orbit coupling and, on the other hand, the valley pseudospin and valleyspin-orbit coupling.^{7–10} In the present work we discuss the *universal* spin dynamics characterizing a diverse range of systems in reduced dimensions, starting from the familiar fully relativistic Dirac equation and a (simplified) Kane model^{11,12} suited for narrow-gap, high- Z semiconductors such as InAs and InSb, to multivalley systems that include staggered single-layer graphene⁸ and transition metal dichalcogenides^{9,13} (TMDCs) such as MoS₂, WS₂, MoS₂ and WSe₂. Indeed, all these systems are characterized by the same generic effective 4×4 Hamiltonian, indicating that we get analogous manifestations of real-spin and valley-pseudospin dynamics. For concreteness, we focus on examples in quasi-1D quantum wires.

This paper is organized as follows. In Sec. II, we discuss the formulation of the generic effective Hamiltonian,

where for different physical systems represented by this Hamiltonian the spin operator matches the real spin, the valley spin or an entangled combination of both the real spin and valley pseudospin. In Sec. III we apply this model to quasi-1D quantum wires, focusing on a range of problems. It has long been debated^{14–18} whether the position operator in a multiband system, when projected on the subspace of positive or negative energies, should acquire a spin-dependent correction that manifests itself as a factor of two for a spin-dependent correction for the velocity operator. Our study suggests that the spin-dependent correction for the position operator and the factor of two in the velocity operator should be absent. We use these results for the velocity operator to discuss equilibrium spin currents in quantum wires.^{19–21} Furthermore, we discuss the Edelstein effect^{22,23} for quantum wires, where an electric field driving a dissipative charge current gives rise to a (pseudo-) spin polarization. Finally, we discuss adiabatic (pseudo-) spin pumping^{24,25} as a means to generate a (pseudo-) spin current. Section VI presents the conclusions.

II. EFFECTIVE 2D HAMILTONIAN

We consider the generic effective 4×4 Hamiltonian in 2D

$$H_{4 \times 4} = H_0 + H_1, \quad (1a)$$

$$H_0 = \frac{1}{2} \Delta \sigma_0 \rho_z, \quad (1b)$$

$$H_1 = \gamma (k_x \sigma_x \rho_x + k_y \sigma_y \rho_x) + e \mathcal{E} \cdot \mathbf{r} \quad (1c)$$

for the motion in a 2D plane. Here ρ_i and σ_i denote Pauli matrices, we have $\sigma_0 = \mathbb{1}_{2 \times 2}$, Δ is the energy gap, $\hbar \mathbf{k} = -i \hbar \nabla + e \mathbf{A}$ is the operator of (crystal) kinetic momentum, and $e \mathcal{E} \cdot \mathbf{r}$ is the potential due to an electric field \mathcal{E} . More explicitly, we have

$$H_{4 \times 4} = \begin{pmatrix} \frac{\Delta}{2} & & & \gamma k_- \\ & \frac{\Delta}{2} & \gamma k_+ & \\ & \gamma k_- & -\frac{\Delta}{2} & \\ \gamma k_+ & & & -\frac{\Delta}{2} \end{pmatrix} + e \mathcal{E} \cdot \mathbf{r}_{4 \times 4} \quad (2a)$$

with $k_{\pm} \equiv k_x \pm ik_y$ and $\mathbf{r}_{n \times n} \equiv \mathbf{r} \mathbb{1}_{n \times n}$, which is unitarily equivalent to

$$\tilde{H}_{4 \times 4} = \begin{pmatrix} H_{2 \times 2} & 0 \\ 0 & H_{2 \times 2}^* \end{pmatrix} \quad (2b)$$

with

$$H_{2 \times 2} = \frac{\Delta}{2} \rho_z + \gamma (k_x \rho_x + k_y \rho_y) + e\mathcal{E} \cdot \mathbf{r}_{2 \times 2}, \quad (3)$$

indicating that the motion of (pseudo-) spin up is completely decoupled from spin down.

The two-band Hamiltonian (1) applies to a range of systems. In all examples discussed in the following, the Pauli matrices ρ_i define the subspaces of positive and negative energies and their off-diagonal couplings, whereas the matrices σ_i represent a spin or pseudospin degree of freedom acting within these bands. The first realization of $H_{4 \times 4}$ is the Dirac Hamiltonian for systems confined to a 2D plane, where $\Delta = 2mc^2$ and $\gamma = \hbar c$. In this case, the matrices σ_i represent the real spin.

Second, $H_{4 \times 4}$ represents a simple version of the Kane Hamiltonian^{11,12} for semiconductor systems in reduced dimensions, where the upper (lower) band in Eq. (1) characterized via the matrices ρ_i becomes the conduction (valence) band separated by the fundamental gap Δ , while σ_i represents the real spin and γ becomes Kane's momentum matrix element (apart from a prefactor $\sqrt{2/3}$). This model is particularly suited for electron systems in narrow-gap materials like InAs and InSb.

Third, the same Hamiltonian applies to staggered single-layer graphene, where γ/\hbar becomes the Fermi velocity and Δ characterizes the sublattice staggering.⁸ Just like in the Kane model, the Pauli matrices ρ_i characterize the conduction and valence bands, yet σ_i represents the valley pseudospin. The real spin and spin-orbit coupling can often be ignored in graphene.⁴

Lastly, the model (1) can be applied to single layers of TMDCs^{9,13} such as MoS₂ and WS₂. Unlike graphene, the larger spin-orbit coupling due to the transition metals' high atomic number gives rise to a significant valley-dependent spin splitting in the valence and (to a lesser extent) in the conduction band. For each band $i = v, c$, these splittings are of the form $\lambda_i \Sigma_z^{(v)} \Sigma_z^{(s)}$, where $\Sigma_z^{(v)}$ ($\Sigma_z^{(s)}$) is a Pauli matrix acting in valley pseudospin (real spin) space. The resulting band structure is depicted in Fig. 1. The system can thus be described by two decoupled replicas $H_{4 \times 4}^{\pm}$ of the Hamiltonian (1) (corresponding to the red and green lines in Fig. 1 and apart from a constant energy shift between the replicas) with gaps $\Delta^{\pm} = \Delta' \pm (\lambda_v + \lambda_c)$, where Δ' denotes the fundamental gap in the absence of SO coupling. In this case, the Pauli matrices σ_i in Eq. (1) represent an entangled combination of real spin and valley pseudospin. Depending on the position of the Fermi energy relative to the bands in Fig. 1, a complete description of TMDCs via Eq. (1) must take into account one or both replicas $H_{4 \times 4}^{\pm}$. For brevity, we drop in the following the superscript \pm , assuming $\Delta = \Delta^+$ or Δ^- .

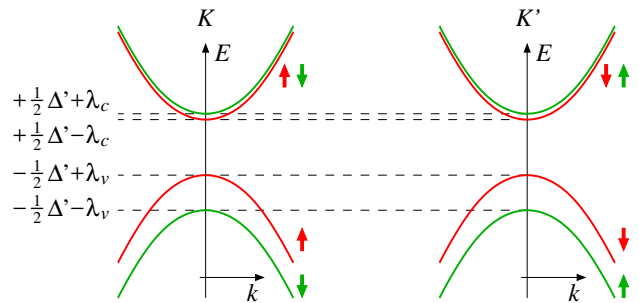


FIG. 1. Energy dispersion near the points K and K' for the lowest conduction and highest valence band in MoS₂. Here Δ' is the fundamental gap in the absence of SO coupling and λ_c (λ_v) is the spin splitting in the conduction (valence) band. The bands marked in red and green thus correspond to decoupled replicas of Hamiltonian (1) with gaps $\Delta^{\pm} = \Delta' \pm (\lambda_v + \lambda_c)$. It was found in Ref. 13 that for WS₂ the sign of λ_c is opposite to the sign in MoS₂ so that the ordering of the spin-split conduction bands near K and K' relative to the ordering of the spin-split valence bands is opposite to the one shown here.

TABLE I. System parameters for the different realizations of the Hamiltonian (1). Numeric values are approximate.

	Δ (eV)	γ (eVÅ)	μ (eVÅ ²)	$-\alpha/\mathcal{E}_y$ (eÅ ²)
Dirac	1.0×10^6	2.0×10^3	7.6	3.7×10^{-6}
InAs ^a	0.42	8.4	3.3×10^2	4.0×10^2
InSb ^a	0.24	8.1	5.5×10^2	1.1×10^3
graphene ^b	~ 0.1	6.6	8.7×10^2	4.3×10^3
MoS ₂ ^c	1.7	3.5	1.4×10^1	4.2
WS ₂ ^c	1.8	4.4	2.2×10^1	6.0
MoSe ₂ ^c	1.5	3.1	1.3×10^1	4.3
WSe ₂ ^c	1.6	3.9	1.9×10^1	5.9

^a Ref. 12

^b Refs. 4 and 8

^c Ref. 9

The material-dependent parameters Δ and γ for the various systems are listed in Table I. The numeric values are approximate. The main purpose of this table is to illustrate the range of numeric values of the parameters Δ and γ characterizing the different systems described by the Hamiltonian (1). Evidently, the generic Hamiltonian $H_{4 \times 4}$ provides a unified treatment of the physics in these systems, despite the rather different numeric values of the model parameters and the different meanings of the (pseudo-) spin σ . Quite generally, any observable physics emerging from the Hamiltonian (1) for one of these systems has a counterpart in the other systems.

In the Hamiltonian $H_{4 \times 4} = H_0 + H_1$ the dynamics of the subspaces of positive and negative energies are coupled via the off-diagonal terms in $H_{4 \times 4}$. The Foldy-Wouthuysen (FW) transformation²⁶ (see also Refs. 12 and 27) is a unitary transformation e^{-S} constructed by successive approximations for the anti-Hermitian operator $S = -S^\dagger$ such that $H_{4 \times 4}^{\text{FW}} \equiv e^{-S} H_{4 \times 4} e^S$ becomes

block-diagonal. This procedure, which is also known as quasi-degenerate perturbation theory, relies on the fact that we may treat H_0 as unperturbed Hamiltonian and H_1 as perturbation. In third order, this yields the block-diagonal Hamiltonian

$$H_{4 \times 4}^{\text{FW}} \equiv e^{-S} H_{4 \times 4} e^S = \begin{pmatrix} \mathcal{H}_+ & 0 \\ 0 & \mathcal{H}_- \end{pmatrix} \quad (4)$$

with effective 2×2 Hamiltonians

$$\begin{aligned} \mathcal{H}_{\pm} &= \left(\pm \frac{\Delta}{2} + e\mathcal{E} \cdot \mathbf{r} \right) \sigma_0 + \frac{\gamma^2}{\Delta} (\pm k^2 \sigma_0 + \frac{e}{\hbar} B_z \sigma_z) \\ &\mp \frac{e\gamma^2}{\Delta^2} (k_x \mathcal{E}_y - k_y \mathcal{E}_x) \sigma_z, \end{aligned} \quad (5)$$

where we used $[r_i, k_j] = i\delta_{ij}$ and $[k_x, k_y] = -\frac{ie}{\hbar} B_z$. By definition of the FW transformation, the subspace of positive energies in Eq. (4) characterized by \mathcal{H}_+ is decoupled from the subspace of negative energy characterized by \mathcal{H}_- so that \mathcal{H}_+ and \mathcal{H}_- can be discussed separately. We also note that the problem exhibits electron-hole symmetry, yet for definiteness we will focus in the following on the subspace with positive energies.

III. EFFECTIVE HAMILTONIAN FOR QUASI-1D QUANTUM WIRE

We illustrate the universal dynamics characterizing the different realizations of the Hamiltonians (1) and (5) by considering a quasi 1D wire along the x direction. Here, ignoring the quantized motion perpendicular to the wire and restricting ourselves to $B_z = 0$, the effective Hamiltonian (5) becomes

$$\mathcal{H} = \frac{1}{2} \mu k^2 + \alpha k \sigma_z, \quad (6)$$

where k is the wave vector along the direction of the wire (dropping the subscript x). From Eq. (5), we have $\mu = 2\gamma^2/\Delta$. The second term in Eq. (6) is a Rashba-type spin splitting²⁸ with $\alpha = -(e\gamma^2/\Delta^2)\mathcal{E}_y$ proportional to the electric field \mathcal{E}_y perpendicular to the wire, which is tunable via external gates.²⁹

For later reference, we summarize some basic properties of quasi-1D electron systems described by the effective Hamiltonian (6). The spin-dependent dispersion becomes

$$E_{\lambda}(k) = \frac{1}{2} \mu k^2 + \lambda \alpha k, \quad (7)$$

where $\lambda = \pm$ characterizes the two (pseudo-) spin subbands. The number density of electrons is given by

$$N_{\lambda} = \int_{-\infty}^{\infty} \frac{dk}{2\pi} f(E), \quad (8)$$

where $f(E)$ is the distribution function. In the following, we consider the limiting cases temperature $T = 0$, when f

is a step function, and high temperature, when f becomes the Maxwell-Boltzmann distribution

$$f(E) = \begin{cases} \theta(E_F - E), & T = 0 \\ e^{-E/k_B T}, & \text{high } T. \end{cases} \quad (9)$$

For $T = 0$ and a given Fermi energy E_F , the Fermi wave vectors for the dispersion (7) become

$$k_{F,\lambda}^{(\pm)} = \pm \sqrt{k_F^2 + \frac{\alpha^2}{\mu^2} - \frac{\lambda\alpha}{\mu}}, \quad (10)$$

where $k_F \equiv \sqrt{2E_F/\mu}$. Assuming small spin-orbit coupling $|\alpha/\mu k_F| \ll 1$, Eq. (10) reduces to

$$k_{F,\lambda}^{(\pm)} \approx \pm k_F - \frac{\lambda\alpha}{\mu} \quad (11)$$

so that the number density in equilibrium becomes

$$N_{\lambda}^{\text{eq}} = \frac{1}{2\pi} [k_{F,\lambda}^{(+)} - k_{F,\lambda}^{(-)}] \approx \frac{k_F}{\pi}. \quad (12)$$

Similarly, at high temperature we define the thermal wave vector $k_T \equiv \sqrt{\pi k_B T / 2\mu}$. Then, assuming $|\alpha/\mu k_T| \ll 1$, we obtain

$$N_{\lambda}^{\text{eq}} = \frac{k_T}{\pi}. \quad (13)$$

IV. POSITION AND VELOCITY OPERATORS

The position and velocity operators in multiband systems such as those described by the Hamiltonian of Eq. (1) are important quantities for a wide range of topics, some of which will be discussed below. It has long been debated¹⁴⁻¹⁸ whether the position operator in a multiband system, when reduced to the subspace of a single band, should acquire a spin-dependent correction that leads to a doubling of the spin-dependent correction for the corresponding velocity operator. We review this question for the particular example of the universal Hamiltonians (1), (5), and (6). Based on our findings, we argue that the spin-dependent correction for the single-band position operator, and the contribution to the single-band velocity operator arising from it, should be absent.³⁰

According to the Heisenberg equation of motion for the position operator $\mathbf{r}_{4 \times 4}$, the velocity operator for the Hamiltonian $H_{4 \times 4}$ becomes^{31,32}

$$\mathbf{v}_{4 \times 4} = \frac{d\mathbf{r}_{4 \times 4}}{dt} = \frac{i}{\hbar} [H_{4 \times 4}, \mathbf{r}_{4 \times 4}] = \frac{\partial H_{4 \times 4}}{\hbar \partial \mathbf{k}} = \frac{\gamma}{\hbar} \boldsymbol{\sigma} \rho_x. \quad (14)$$

On the other hand, we may define the velocity operator for the effective 2×2 Hamiltonian \mathcal{H}_+ in two different ways. In the first approach, we use

$$\mathbf{v}_{2 \times 2} = \frac{i}{\hbar} [\mathcal{H}_+, \mathbf{r}_{2 \times 2}] = \frac{\partial \mathcal{H}_+}{\hbar \partial \mathbf{k}} = \frac{1}{\hbar} \left(\frac{2\gamma^2}{\Delta} \mathbf{k} - \frac{\gamma^2}{\Delta^2} \boldsymbol{\mathcal{E}} \times \boldsymbol{\sigma} \right). \quad (15)$$

In the second approach, we remember the fact that \mathcal{H}_+ was derived via a FW transformation e^{-S} from the Hamiltonian $H_{4 \times 4}$. Accordingly, we first apply the same unitary transformation to $\mathbf{r}_{4 \times 4}$, which yields

$$\mathbf{r}_{4 \times 4}^{\text{FW}} \equiv e^{-S} \mathbf{r}_{4 \times 4} e^S, \quad (16a)$$

$$= \mathbf{r}_{4 \times 4} + \frac{\gamma^2}{\Delta^2} \mathbf{k} \times \boldsymbol{\sigma} \rho_0 - \frac{\gamma}{\Delta} \boldsymbol{\sigma} \rho_y, \quad (16b)$$

$$= \begin{pmatrix} \mathbf{r}_{2 \times 2}^{\text{FW}} & \frac{i\gamma}{\Delta} \boldsymbol{\sigma} \\ -\frac{i\gamma}{\Delta} \boldsymbol{\sigma} & \mathbf{r}_{2 \times 2}^{\text{FW}} \end{pmatrix}. \quad (16c)$$

Unlike the transformed Hamiltonian $H_{4 \times 4}^{\text{FW}}$, the transformed FW position operator $\mathbf{r}_{4 \times 4}^{\text{FW}}$ does not acquire a block-diagonal form. Ignoring the off-diagonal part that couples the subspaces of positive and negative energies, we get the following modified FW position operator for the subspace of \mathcal{H}_+

$$\mathbf{r}_{2 \times 2}^{\text{FW}} = \mathbf{r}_{2 \times 2} + \frac{\gamma^2}{\Delta^2} \mathbf{k} \times \boldsymbol{\sigma}. \quad (17)$$

Alluding to Ref. 14, the spin-dependent part of $\mathbf{r}_{2 \times 2}^{\text{FW}}$ has sometimes been called the Yafet term.¹⁷ The modified FW position operator yields the velocity operator

$$\mathbf{v}_{2 \times 2}^{\text{FW}} = \frac{i}{\hbar} [\mathcal{H}_+, \mathbf{r}_{2 \times 2}^{\text{FW}}] = \frac{1}{\hbar} \left(\frac{2\gamma^2}{\Delta} \mathbf{k} - \frac{2\gamma^2}{\Delta^2} \boldsymbol{\mathcal{E}} \times \boldsymbol{\sigma} \right). \quad (18)$$

The same result (18) is obtained if the FW transformation is applied to the velocity operator $\mathbf{v}_{4 \times 4}$, which yields³³

$$\mathbf{v}_{4 \times 4}^{\text{FW}} \equiv e^{-S} \mathbf{v}_{4 \times 4} e^S, \quad (19a)$$

$$= \frac{1}{\hbar} \left[\frac{2\gamma^2}{\Delta} \mathbf{k} - \frac{2\gamma^2}{\Delta^2} \boldsymbol{\mathcal{E}} \times \boldsymbol{\sigma} \rho_0 + \gamma \boldsymbol{\sigma} \rho_x + \frac{\gamma^3}{\hbar \Delta^2} \mathbf{k} (\mathbf{k} \cdot \boldsymbol{\sigma}) \rho_x \right], \quad (19b)$$

$$= \begin{pmatrix} \mathbf{v}_{2 \times 2}^{\text{FW}} & \frac{\gamma}{\hbar} \boldsymbol{\sigma} + \frac{\gamma^3}{\hbar \Delta^2} \mathbf{k} (\mathbf{k} \cdot \boldsymbol{\sigma}) \\ \frac{\gamma}{\hbar} \boldsymbol{\sigma} + \frac{\gamma^3}{\hbar \Delta^2} \mathbf{k} (\mathbf{k} \cdot \boldsymbol{\sigma}) & \mathbf{v}_{2 \times 2}^{\text{FW}} \end{pmatrix}. \quad (19c)$$

Ignoring the off-diagonal blocks we reproduce Eq. (18). Comparing Eqs. (15) and (18) we see that the spin-dependent parts characterizing $\mathbf{v}_{2 \times 2}$ and $\mathbf{v}_{2 \times 2}^{\text{FW}}$ differ by a factor of two. The significance of this factor of two has been debated in the past.^{14–18}

Focusing on quasi-1D wires discussed here, the Hellmann-Feynman theorem applied to Eq. (14) yields

$$\langle v_{4 \times 4} \rangle(k) = \left\langle \frac{\partial H_{4 \times 4}}{\partial k} \right\rangle = \frac{\partial E_{\lambda, 4 \times 4}}{\hbar \partial k}, \quad (20)$$

where the expectation value is taken for the 4-component wire eigenstates of $H_{4 \times 4} + V(y) \sigma_0 \rho_z$ with eigenvalues $E_{\lambda, 4 \times 4}(k)$, and $V(y)$ is the confining potential of the quantum wire. Accordingly, the expectation value $\langle v_{4 \times 4} \rangle$ as a function of k changes sign at the extrema of the

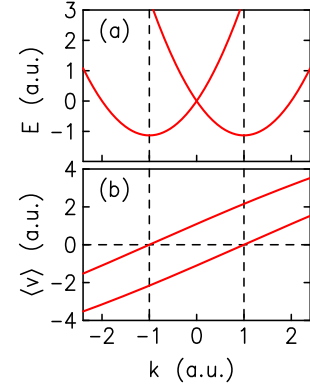


FIG. 2. (a) Spin-split dispersion and (b) expectation value of the velocity $v_{4 \times 4}$ for a quantum wire described by the 4×4 Hamiltonian (1) augmented by an inversion-asymmetric mass confinement in y direction. The numerical results shown here were obtained using the quadrature method described in Ref. 34.

dispersion $E_{\lambda, 4 \times 4}(k)$. This is illustrated in Fig. 2 for a quasi-1D wire realized via an inversion-asymmetric confinement $V(y)$. On the other hand, the 2×2 model (6) yields

$$v = [\mathcal{H}, x] = \frac{\partial \mathcal{H}}{\hbar \partial k} = \frac{1}{\hbar} (\mu k + \alpha \sigma_z), \quad (21a)$$

$$v^{\text{FW}} = [\mathcal{H}, x^{\text{FW}}] = \frac{1}{\hbar} (\mu k + 2\alpha \sigma_z). \quad (21b)$$

Thus an important difference between v and v^{FW} lies in the fact that the extrema of the dispersion (7) at $k_{0, \lambda} \equiv -\lambda \alpha / \mu$ are characterized by $\langle v \rangle(k_{0, \lambda}) = 0$, but $\langle v^{\text{FW}} \rangle(k_{0, \lambda}) \neq 0$.

The FW transformation e^{-S} is set up with the goal to yield the Hamiltonian for the effective one-band model that faithfully reproduces the features of the full two-band theory at low energies. Assuming that the relation (20) between velocity and dispersion should also hold for a system described by the one-band Hamiltonian (6), the Hellmann-Feynman theorem implies

$$\langle v \rangle(k) = \frac{\partial E_{\lambda}}{\hbar \partial k} = \left\langle \frac{\partial \mathcal{H}}{\hbar \partial k} \right\rangle, \quad (22)$$

where the expectation value is now taken for the 2-component eigenstates of \mathcal{H} with eigenvalues $E_{\lambda}(k)$. Comparing Eq. (22) with Eq. (21), we conclude that only v is consistent with Eq. (20), i.e., for both the two-band Hamiltonian (1) and the one-band Hamiltonians (5) and (6) the position operator should not include a spin-dependent term. We speculate that the discrepancy between the predictions from v^{FW} and Eq. (20) may be due to the fact that the approximate FW transformation e^{-S} used to derive $\mathbf{v}_{2 \times 2}^{\text{FW}}$ from $\mathbf{v}_{4 \times 4}$ (and $\mathbf{r}_{2 \times 2}^{\text{FW}}$ from $\mathbf{r}_{4 \times 4}$) is applied to *operators* so that it is generally difficult to estimate the magnitude of the omitted terms.³¹ Note that the terms omitted when going from Eq. (19) to Eq. (18) include the original Dirac velocity operator

(14) whose matrix elements may contribute substantially to expectation values.

V. UNIVERSAL (PSEUDO-) SPIN DYNAMICS IN QUASI-1D QUANTUM WIRES

In the following we discuss a few examples for the universal (pseudo-) spin dynamics in quasi-1D quantum wires emerging from the Hamiltonian (6).

A. Equilibrium Spin Currents

Using Rashba's definition,¹⁹ the spin current operator for the velocity operator v in Eq. (21) becomes

$$j_s \equiv \{v, \sigma_z\} = \frac{1}{\hbar} (\mu k \sigma_z + \alpha), \quad (23)$$

where $\{A, B\} \equiv \frac{1}{2} (AB + BA)$. The total average spin current is obtained using

$$I_s = \langle j_s \rangle = \langle \{v, \sigma_z\} \rangle = \sum_{\nu=\pm} \int \frac{dk}{2\pi} \langle \nu | \{v, \sigma_z\} | \nu \rangle. \quad (24)$$

Equation (7) shows that the parabolic dispersion curves for the two spin subbands are centered about $-\lambda\alpha/\mu$ [Fig. 3(a)]. As expected,^{20,21} this yields $\langle j_s \rangle = 0$. This holds for both $T = 0$ and high temperatures.

For comparison, we note that the spin current for the modified FW velocity operator becomes

$$j_s^{\text{FW}} = \{v^{\text{FW}}, \sigma_z\} = \frac{1}{\hbar} (\mu k \sigma_z + 2\alpha) = j_s + \alpha/\hbar. \quad (25)$$

For both $T = 0$ and high temperatures, the total equilibrium spin current (24) then becomes $(\alpha/\hbar)N^{\text{eq}}$, where $N^{\text{eq}} = N_+^{\text{eq}} + N_-^{\text{eq}}$ is the total electron density in equilibrium given by Eq. (8).

B. Edelstein Effect

We consider a driving electric field \mathcal{E}_x along the direction of the wire. In a dissipative regime, using a Drude model,³⁵ the distribution is then shifted from $f(k)$ to $f[k + k_\nu^d(k)]$, where $k_\nu^d(k) = e\mathcal{E}_x\tau_\nu(k)/\hbar$. This causes a net motion of electrons depicted in Fig. 3(b), where more spin-up states contribute to the charge current than spin-down states. This phenomenon resulting in a net spin polarization is often called the Edelstein effect,²² see also Refs. 23 and 36. Here we evaluate the Edelstein effect for a quasi-1D quantum wire characterized by the generic Hamiltonian (6). Recently, a valley Edelstein effect in 2D systems has been discussed in Ref. 37.

We express the scattering time τ_ν as a power law³⁸

$$\tau_\nu(k) = \zeta_\nu k^{2\nu}, \quad \nu = 0, 1, 2, \quad (26)$$

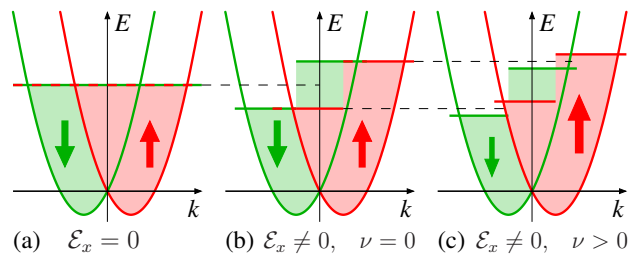


FIG. 3. Qualitative sketch of the dispersion $E(k)$ of a quantum wire with Rashba-like SO coupling at $T = 0$ (a) in thermal equilibrium with electric field $\mathcal{E}_x = 0$, (b) in the presence of a driving electric field $\mathcal{E}_x > 0$ along the wire and a dissipative regime with $\nu = 0$ and (c) $\mathcal{E}_x > 0$ with $\nu > 0$. Horizontal colored lines indicate the quasi Fermi levels for left and right movers in the two spin subbands. In (a) and (b) the net spin polarization and the spin current are exactly zero. In (c) the driving electric field results in a steady state with a net spin polarization (Edelstein effect).

where ζ_ν is a proportionality constant. The parameter ν depends on the scattering mechanism.^{23,38} Scattering by, e.g., acoustic and optical phonons and screened ionized impurities corresponds to the case $\nu = 0$. The case $\nu = 1$ pertains to piezoelectric scattering by acoustic phonons or scattering by polar optical phonons. Scattering by weakly screened ionized impurities belongs to the case $\nu = 2$. We define the net spin polarization as

$$\mathcal{P} = \frac{N_+ - N_-}{N_+ + N_-}, \quad (27)$$

where N_λ is the number density for each spin subband λ . As expected, in thermal equilibrium ($\mathcal{E}_x = 0$) we have $\mathcal{P} = 0$ [Fig. 3(a)].

1. Zero Temperature

In the zero temperature case with driving electric field, the distribution becomes a shifted step function. For a weak electric field \mathcal{E}_x , we can assume that $|k_\nu^d(k_F)/k_F| \ll 1$ so that the extremal wave vectors for the occupied states are approximately

$$k^{(\pm)} = k_{F,\lambda}^{(\pm)} - k_\nu^d(k_{F,\lambda}^{(\pm)}). \quad (28)$$

This yields quasi Fermi levels for left and right movers in the two spin subbands

$$E_{F,\lambda}^{(\pm)} = E_F + \frac{ek_F^{2\nu}\mathcal{E}_x\zeta_\nu}{\hbar} (\mp\mu k_F + 2\lambda\nu\alpha), \quad (29)$$

where we assumed small SO coupling $|\alpha/\mu k_F| \ll 1$. Thus we have two contributions for the \mathcal{E}_x -dependent corrections to the quasi-Fermi levels $E_{F,\lambda}^{(\pm)}$: a spin-independent correction $\propto \mp k_F$ raises E_F for the right movers and lowers E_F for the left movers. For $\nu > 0$, the spin-dependent correction $\propto \lambda\nu\alpha$ is positive for both right-

and left movers in one spin subband, and it is negative for the other spin subband, corresponding to a transfer of electrons from one spin subband to the other.

The Edelstein effect also becomes explicit by looking at the number densities N_λ as a function of driving field \mathcal{E}_x . For small SO coupling $|\alpha/\mu k_F| \ll 1$ we get

$$N_\lambda = N_\lambda^{\text{eq}} \left[1 + \lambda \frac{2\nu\alpha k_\nu^d(k_F)}{\mu k_F^2} \right] \quad (30)$$

and the polarization for any ν is

$$\mathcal{P} = 2\nu \frac{\alpha k_\nu^d(k_F)}{\mu k_F^2}. \quad (31)$$

The trivial case $\nu = 0$ is one where the scattering time τ is a constant independent of the wave vector k . As can be seen in Eq. (30), the number densities for spin up and spin down subbands are equal, which means that there is no net spin polarization, $\mathcal{P} = 0$. This also means that a constant shift k_0^d in the electron distribution does not affect the number density in each subband. On the other hand, an unequal shift in the wave vector $k^{(+)}$ and $k^{(-)}$ results in an imbalance among spin-up and spin-down states, yielding a nonzero spin polarization.

We define the average scattering time $\bar{\tau}_\nu$ for any ν as²³

$$\bar{\tau}_\nu = \frac{\langle \tau_\nu E \rangle}{\langle E \rangle}, \quad (32)$$

where for a function ϕ , the average $\langle \phi \rangle$ is defined as

$$\langle \phi \rangle = \frac{\int_{-\infty}^{+\infty} \phi(k) f(k) dk}{\int_{-\infty}^{+\infty} f(k) dk}. \quad (33)$$

We also define $\bar{k}_\nu^d \equiv e\mathcal{E}_x\bar{\tau}_\nu/\hbar$ so that Eq. (31) can then be written generally as²³

$$\mathcal{P} = Q \frac{\alpha \bar{k}_1^d}{\langle E \rangle}, \quad (34)$$

where Q is a dimensionless number that depends on ν . Its value for the different limiting temperatures are listed in Table II.

2. High Temperature

Similar to the case $T = 0$, we can derive the number density for each spin subband, and hence the spin polarization at high temperature by shifting the Maxwell-Boltzmann distribution in Eq. (9) by $k_\nu^d(k)$. Again we assume small spin-orbit coupling $|\alpha/\mu k_T| \ll 1$ and weak electric fields $|k_\nu^d(k_T)/k_T| \ll 1$. The number density then simplifies to

$$N_\lambda = N_\lambda^{\text{eq}} \left[1 + \lambda \frac{\pi k_\nu^d(k_T)}{k_T} \left(\frac{4}{\pi} \right)^\nu \frac{\nu(2\nu-1)!!}{2^\nu} \frac{\alpha}{\mu k_T} \right], \quad (35)$$

TABLE II. Numerical value for Q at the limiting temperatures for $\nu = 0, 1, 2$.

Q	$T = 0$	high T
$\nu = 0$	0	0
$\nu = 1$	5/9	1/3
$\nu = 2$	14/9	2/5

which yields the polarization

$$\mathcal{P} = \frac{\pi\alpha k_\nu^d(k_T)}{\mu k_T^2} \left(\frac{4}{\pi} \right)^\nu \frac{\nu(2\nu-1)!!}{2^\nu}. \quad (36)$$

Similar to zero temperature, the case $\nu = 0$ gives the same number densities for both spin subbands [see Eq. (35)] so that $N_+ - N_- = 0$ and hence $\mathcal{P} = 0$. For the cases $\nu = 1, 2$, we obtain a polarization of the form (34) with values of Q listed in Table II.

C. Adiabatic (Pseudo-) Spin Pumping

In quantum wires obeying the Hamiltonian (6), dc spin currents can be generated via parametric pumping,^{24,25} where one varies periodically a potential barrier V_{bar} in the wire and the electric field perpendicular to it (Fig. 4). Here the total Hamiltonian becomes

$$H = \mathcal{H} + V_{\text{bar}}. \quad (37)$$

Assuming that the potential barrier is a δ potential, $V_{\text{bar}} = V\delta(x)$, the spin- λ particle current is derived using the parametric integral²⁴

$$I_\lambda = \frac{\omega}{2\pi^2} \int_A dV d\alpha \text{Im} \left(\frac{\partial r_\lambda^*}{\partial V} \frac{\partial r_\lambda}{\partial \alpha} + \frac{\partial t_\lambda^*}{\partial V} \frac{\partial t_\lambda}{\partial \alpha} \right), \quad (38)$$

where r_λ and t_λ are the reflection and transmission coefficients, respectively, for particles with (pseudo-) spin λ , and the integral is over the area A enclosed by the path in the parameter space (V, α) . For a sinusoidal pumping cycle with $V = V_0 + \Delta V \sin(\omega t)$ and $\alpha = \alpha_0 + \Delta\alpha \sin(\omega t - \phi)$ and assuming the weak-pumping limit $\Delta V \ll V_0$ and $\Delta\alpha \ll \alpha_0$, the total spin current $I_s = I_+ - I_-$ becomes²⁵

$$I_s = \frac{\omega}{\pi} \sin(\phi) \Delta V \Delta\alpha \frac{\mu k_F^2 L V_0}{(\mu^2 k_F^2 + V_0^2)^2} \quad (39a)$$

$$\equiv I_s^{(0)} \omega \sin(\phi) \frac{\Delta V}{V_0} \frac{\Delta\alpha}{\alpha_0} \quad (39b)$$

with dimensionless prefactor

$$I_s^{(0)} = \frac{1}{\pi} \frac{\mu k_F^2 L V_0^2 \alpha_0}{(\mu^2 k_F^2 + V_0^2)^2}, \quad (39c)$$

where L is the length of the region of the wire and α is modulated by tuning the field \mathcal{E}_y (Fig. 4). The maximum

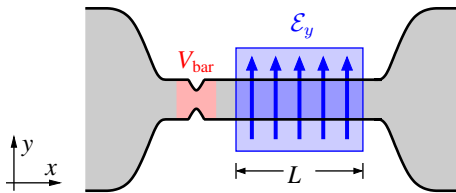


FIG. 4. Schematic diagram for an adiabatic (pseudo-) spin pump.²⁵ A potential barrier V_{bar} is present at the left end of the wire. A perpendicular electric field \mathcal{E}_y is applied in the blue shaded region of length L in order to tune the coupling coefficient $\alpha \propto \mathcal{E}_y$.

spin current is achieved when $V_0 \simeq \mu k_F$, which corresponds to a barrier $V_0 \delta(x)$ with transmission probability $T \simeq 1/2$. Also, this corresponds to a maximum $I_s^{(0)}$

$$I_s^{(0),\text{max}} \simeq \frac{eL\mathcal{E}_y}{8\pi\Delta}, \quad (40)$$

implying that only the energy gap Δ characterizes the materials' effectiveness for operating a (valley) spin pump. In particular, $I_s^{(0),\text{max}}$ is independent of the Fermi wave vector or density. For a length $L \simeq 10 \mu\text{m}$ and lateral electric field $\mathcal{E}_y \simeq 1 \text{ kV/cm}$, we have $I_s^{(0),\text{max}} \simeq 0.1$ for InAs, InSb and graphene and $I_s^{(0),\text{max}} \simeq 0.01$ for TMDCs. For frequencies $\omega \simeq 10^4 - 10^5 \text{ s}^{-1}$ and $\frac{\Delta V}{V_0} \frac{\Delta\alpha}{\alpha_0} \simeq 0.1$, the spin current becomes $I_s \simeq 100 \text{ s}^{-1}$, which is comparable to the charge currents in single-electron transistors.³⁹

Equation (39) represents a scheme to generate spin currents in a quantum wire that relies on adiabatic pumping.^{24,25} An alternative scheme operating in a dissipative regime and likewise applicable to the different realizations of the Hamiltonian (6) was discussed in Ref. 20.

VI. CONCLUSION

In this work we showed that a general effective Hamiltonian can be formulated to describe spin-dependent phenomena in low-dimensional systems that is realized in a range of different materials. The spin σ_i appearing in Hamiltonian (1) corresponds to the real spin in Dirac

or Kane systems, whereas it represents the valley pseudospin in graphene and a combination of valley and real spins in TMDCs. The universal nature of the Hamiltonian (1) implies that the spin dynamics present in one of these systems exists similarly in the other systems realizing Hamiltonian (1). On a qualitative level, the universality of the dynamics is not affected by perturbations such as (pseudo) spin relaxation, while specific numbers for the various systems are certainly different as illustrated by the material parameters listed in Table I. Projecting the two-band Hamiltonian (1) on the conduction or valence band yields the effective single-band Hamiltonian (5). In order to describe quasi-1D systems the latter can be further simplified, yielding Eq. (6).

A comparison between the effective one-band Hamiltonian (6) and the more complete two-band Hamiltonian (1) allowed us to identify the correct form of the (pseudo-) spin-dependent velocity operator to be used in a single-band theory. We have shown that equilibrium (pseudo-) spin currents vanish in quasi-1D systems governed by the Hamiltonian (6). We have also studied the Edelstein effect for quantum wires, whereby in a dissipative regime a driving electric field induces a (pseudo-) spin polarization. This effect vanishes in quasi-1D wires where the scattering time τ is independent of the wave vector k . For $\tau \propto k^{2\nu}$, $\nu \geq 0$, the spin polarization is given by Eq. (34). Lastly, we considered adiabatic spin pumping in quasi-1D wires. The induced spin current can be optimized by choosing a critical barrier strength $V_0 \simeq \mu k_F$. For realistic values of system parameters, the maximum spin current is $I_s \simeq 100 \text{ s}^{-1}$. We have only presented here a limited number of examples illustrating the universal (pseudo-) spin dynamics in low-dimensional systems emerging from the generic Hamiltonian (1). More examples can be identified.

ACKNOWLEDGMENTS

We appreciate stimulating discussions with G. Burkard, D. Culcer, M. Governale, A. Kormányos, Q. Niu, E. Rashba, and D. Xiao. RW appreciates the hospitality of Victoria University of Wellington, where part of this work was performed. This work was supported by the NSF under grant No. DMR-1310199. Work at Argonne was supported by DOE BES under Contract No. DE-AC02-06CH11357.

* eafajardo@niu.edu; On leave from: Department of Physics, Mindanao State University-Main Campus, Marawi City, Lanao del Sur, Philippines 9700

¹ S. A. Wolf, D. D. Awschalom, R. A. Buhrman, J. M. Daughton, S. von Molnár, M. L. Roukes, A. Y. Chtchelkanova, and D. M. Treger, *Science* **294**, 1488 (2001).

² I. Žutić, J. Fabian, and S. Das Sarma, *Rev. Mod. Phys.* **76**, 323 (2004).

³ T. Dietl, D. D. Awschalom, M. Kamińska, and H. Ohno, eds., *Spintronics*, vol. 82 of *Semiconductors and Semimetals* (Elsevier, 2008).

⁴ A. H. Castro Neto, F. Guinea, N. M. R. Peres, K. S. Novoselov, and A. K. Geim, *Rev. Mod. Phys.* **81**, 109 (2009).

⁵ Y. P. Shkolnikov, E. P. De Poortere, E. Tutuc, and M. Shayegan, *Phys. Rev. Lett.* **89**, 226805 (2002).

- ⁶ O. Gunawan, Y. P. Shkolnikov, K. Vakili, T. Gokmen, E. P. De Poortere, and M. Shayegan, *Phys. Rev. Lett.* **97**, 186404 (2006).
- ⁷ A. Rycerz, J. Tworzydło, and C. W. J. Beenakker, *Nat. Phys.* **3**, 172 (2007).
- ⁸ D. Xiao, W. Yao, and Q. Niu, *Phys. Rev. Lett.* **99**, 236809 (2007).
- ⁹ D. Xiao, G.-B. Liu, W. Feng, X. Xu, and W. Yao, *Phys. Rev. Lett.* **108**, 196802 (2012).
- ¹⁰ J. R. Schaibley, H. Yu, G. Clark, P. Rivera, J. S. Ross, K. L. Seyler, W. Yao, and X. Xu, *Nat. Mater.* **1**, 16055 (2016).
- ¹¹ E. O. Kane, *J. Phys. Chem. Solids* **1**, 249 (1957).
- ¹² R. Winkler, *Spin-Orbit Coupling Effects in Two-Dimensional Electron and Hole Systems* (Springer, Berlin, 2003).
- ¹³ A. Kormányos, G. Burkard, M. Gmitra, J. Fabian, V. Zólyomi, N. D. Drummond, and V. Fal'ko, *2D Mater.* **2**, 022001 (2015).
- ¹⁴ Y. Yafet, in *Solid State Phys.*, edited by F. Seitz and D. Turnbull (Academic, New York, 1963), vol. 14, pp. 1–98.
- ¹⁵ P. Nozières and C. Lewiner, *J. Phys. (France)* **34**, 901 (1973).
- ¹⁶ E. J. Baerends, W. H. E. Schwarz, P. Schwerdtfeger, and J. G. Snijders, *J. Phys. B: At. Mol. Opt. Phys.* **23**, 3225 (1990).
- ¹⁷ H.-A. Engel, E. I. Rashba, and B. I. Halperin, in *Handbook of Magnetism and Advanced Magnetic Materials*, edited by H. Kronmüller and S. Parkin (Wiley, Chichester, UK, 2007), vol. V, pp. 2858–2877.
- ¹⁸ X. Bi, P. He, E. M. Hankiewicz, R. Winkler, G. Vignale, and D. Culcer, *Phys. Rev. B* **88**, 035316 (2013).
- ¹⁹ E. I. Rashba, *Phys. Rev. B* **68**, 241315 (2003).
- ²⁰ A. G. Mal'shukov, C. S. Tang, C. S. Chu, and K. A. Chao, *Phys. Rev. B* **68**, 233307 (2003).
- ²¹ A. A. Kiselev and K. W. Kim, *Phys. Rev. B* **71**, 153315 (2005).
- ²² V. Edelstein, *Solid State Commun.* **73**, 233 (1990).
- ²³ A. G. Aronov, Y. B. Lyanda-Geller, and G. E. Pikus, *Sov. Phys. JETP* **73**, 537 (1991).
- ²⁴ P. W. Brouwer, *Phys. Rev. B* **58**, R10135 (1998).
- ²⁵ M. Governale, F. Taddei, and R. Fazio, *Phys. Rev. B* **68**, 155324 (2003).
- ²⁶ L. L. Foldy and S. A. Wouthuysen, *Phys. Rev.* **78**, 29 (1950).
- ²⁷ G. L. Bir and G. E. Pikus, *Symmetry and Strain-induced Effects in Semiconductors* (Wiley, New York, 1974).
- ²⁸ Y. A. Bychkov and E. I. Rashba, *JETP Lett.* **39**, 78 (1984).
- ²⁹ J. Nitta, T. Akazaki, H. Takayanagi, and T. Enoki, *Phys. Rev. Lett.* **78**, 1335 (1997).
- ³⁰ The FW transformation has been applied to a wide range of physical systems, see, e.g., M. Wagner, *Unitary Transformations in Solid State Physics* (North-Holland, Amsterdam, 1986). We anticipate that the problem of FW-transformed non-blockdiagonal observables exists for these other systems, too.
- ³¹ B. Thaller, *The Dirac Equation* (Springer, Berlin, 1992).
- ³² R. Winkler, U. Zülicke, and J. Bolte, *Phys. Rev. B* **75**, 205314 (2007).
- ³³ In order to derive $\mathbf{v}_{4 \times 4}^{\text{FW}}$ as in Eq. (19) via the equation of motion $\mathbf{v}_{4 \times 4}^{\text{FW}} = \frac{i}{\hbar} [H_{4 \times 4}^{\text{FW}}, \mathbf{r}_{4 \times 4}^{\text{FW}}]$, it is necessary to evaluate the FW transformation for $\mathbf{r}_{4 \times 4}^{\text{FW}}$ up to *fourth* order.
- ³⁴ R. Winkler and U. Rössler, *Phys. Rev. B* **48**, 8918 (1993).
- ³⁵ R. G. Chambers, *Electrons in Metals and Semiconductors* (Chapman and Hall, London, 1990).
- ³⁶ E. L. Ivchenko and G. E. Pikus, *JETP Lett.* **27**, 604 (1978).
- ³⁷ K. Taguchi, Y. Kawaguchi, Y. Tanaka, and K. T. Law, *Valley Edelstein effect in monolayer transition metal dichalcogenides*, arXiv:1705.08224 (2017).
- ³⁸ J. Kainz, U. Rössler, and R. Winkler, *Phys. Rev. B* **70**, 195322 (2004).
- ³⁹ R. Schleser, E. Ruh, T. Ihn, K. Ensslin, D. C. Driscoll, and A. C. Gossard, *Appl. Phys. Lett.* **85**, 2005 (2004).